TOPOLOGICAL DERIVATIVE IN MULTI-SCALE LINEAR ELASTICITY MODELS APPLIED TO THE SYNTHESIS OF MICROSTRUCTURES

S. AMSTUTZ, S.M. GIUSTI, A.A. NOVOTNY, AND E.A. DE SOUZA NETO

ABSTRACT. This paper proposes an algorithm for the synthesis/optimization of microstructures based on an *exact* formula for the topological derivative of the macroscopic elasticity tensor and a level-set domain representation. The macroscopic elasticity tensor is estimated by a standard multi-scale constitutive theory where the strain and stress tensors are volume averages of their microscopic counterparts over a Representative Volume Element (RVE). The algorithm is of simple computational implementation. In particular, it does not require artificial algorithmic parameters or strategies. This is in sharp contrast with existing microstructural optimization procedures and follows as a natural consequence of the use of the topological derivative concept. This concept provides the correct mathematical framework to treat topology changes such as those characterizing microstuctural optimization problems. The effectivenes of the proposed methodology is illustrated in a set of finite element-based numerical examples.

1. INTRODUCTION

The accurate prediction of the constitutive behaviour of a continuum body under loading is of paramount importance in many areas of engineering and science. Until about a decade ago, this issue has been addressed mainly by means of conventional phenomenological constitutive theories. More recently, the increasing understanding of the microscopic mechanisms responsible for the macroscopic response, allied to the industrial demand for more accurate predictive tools, led to the development and use of so-called multi-scale constitutive theories. Such theories are currently a subject of intensive research in applied mathematics and computational mechanics. Their starting point can be traced back to the pioneering developments reported in [25, 26, 33, 11, 43, 48]. Early applications were concerned with the description of relatively simple micro-scale phenomena often treated by analytical or semi-analytical methods [6, 7, 24, 37, 38, 41]. More recent applications rely often on finite element-based computational simulations [34, 35] and are frequently aplied to more complex material behaviour in areas such as the modelling of human arterial tissue [47], bone [42], the plastic behavior of porous metals [21] and the microstructural evolution and phase transition in the solidification of metals [13].

One interesting branching of such developments is the study of the sensitivity of the macroscopic response to changes in the underlying microstucture. The sensitivity information becomes essential in the analysis and potential purpose-design and optimization of heterogenoues media. For instance, sensitivity information obtained by means of a relaxation-based technique has been successfully used in [2, 30, 31] to design microstructural topologies with negative macroscopic Poisson's ratio. Multi-scale models have also been applied with success to the topology optimization of load bearing structures in the context of the so-called homogenization approach to topology optimization (see, for instance, the review paper by Eschenauer and Olhoff [17]) based on the fundamental papers by Bendsøe and Kikuchi [10] and Zochowski [50]. In such cases, the microscale model acts as a regularization of the exact problem posed by a material point turning into a hole [9]. The homogenization approach has also been applied to microstructural topology optimization problems where the target is the design of topologies that yield pre-specified or extreme macroscopic response [29, 44, 45]. One of the drawbacks of this methodology, however, is that it often produces designs with large regions consisting of perforated material. To deal with this problem, a penalization of intermediate densities is commonly introduced.

In contrast to the homogenization approach, we propose in this paper a microstructural synthesis/optimization algorithm relying on the mathematical concept of *topological derivative* [46, 12, 16] combined with a level-set domain representation. In this context, a (remarkably simple) *exact* formula for the sensitivity of the macroscopic elasticity tensor to the insertion of inclusions at the micro-scale is used. This analytical formula provides a rigorous first order approximation to the variation in the

Key words and phrases. Topological derivative; sensitivity analysis; multi-scale modelling; level-set domain representation; synthesis of microstructures.

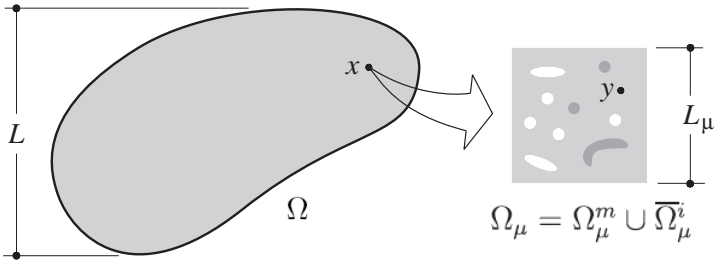

FIGURE 1. Macroscopic continuum with a locally attached microstructure.

macroscopic elasticity tensor resulting from the insertion of a circular inclusion of a given phase contrast. It is derived by making use of the notions of topological asymptotic analysis and topological derivative within the variational formulation of well-established multi-scale constitutive theory [20, 34] where the macroscopic strain and stress tensors are volume averages of their microscopic counterparts over a Representative Volume Element (RVE) of material.

The relatively new concept of topological asymptotic expansion allows the exact calculation of the sensitivity of a given shape functional with respect to infinitesimal domain perturbations such as the insertion of voids, inclusions, source terms or even cracks. It has proved extremely useful in the treatment of a wide range of problems, including the topology optimization of load-bearing structures [1, 4, 39], inverse analysis [5, 18, 27] and image processing [8, 28, 32], and is currently a subject of great interest in applied mathematics circles [3, 19, 36, 49]. In the present context, when combined with the ideas introduced in [4], the use of the exact topological sensitivity formula results in a microstructural optimization algorithm of simple computational implementation. In particular, the algorithm is free from artificial algorithmic parameters and does not require extra post-processing strategies when new topologies are generated throughout its iterations. This is only a natural consequence of the use of the notion of topological derivative which provides the correct mathematical framework for the treatment of the inherently singular changes in topology that characterize microstructural optimization problems. The effectiveness and robustness of the proposed algorithm is illustrated in a number of finite element-based numerical examples of microstructural optimization.

The paper is organized as follows. The multi-scale constitutive framework adopted in the estimation of the macroscopic elasticity tensor is briefly reviewed in Section 2. The concept of topological asymptotic expansion and topological derivative – upon which the algorithm proposed in this paper relies – is briefly reviewed in Section 3 where the closed formula for the topological derivative of the macroscopic elasticity tensor is also presented. The proposed microstructural topology optimization algorithm is presented in Section 4 and the numerical examples are shown in Section 5. The paper closes in Section 6 with some concluding remarks.

2. Multi-scale modelling

The homogenisation-based multi-scale constitutive framework presented, among others, in [20, 34, 35], is adopted here in the estimation of the macroscopic elastic response from the knowledge of the underlying microstructure. The main idea behind this well-established family of constitutive theories is the assumption that any point x of the macroscopic continuum (refer to Fig. 1) is associated to a local Representative Volume Element (RVE) whose domain Ω_μ, with boundary $\partial\Omega_\mu$, has characteristic length L_μ, much smaller than the characteristic length L of the macro-continuum domain Ω.

The axiomatic structure of this family of theories is described in detail in [14, 15] Accordingly, the entire theory can be formally derived on the basis of five basic assumptions: (i) the strain averaging relation; (ii) the requirement that the chosen functional set of kinematically admissible displacement fluctuations of the RVE be a subspace of the minimally constrained space compatible with the strain averaging hypothesis; (iii) the mechanical equilibrium of the RVE; (iv) the stress averaging relation, and; (v) the Hill-Mandel Principle of Macro-Homogeneity [26, 33], which ensures the energy consistency between the so-called micro- and macro-scales.

Assumption (i) uses the concept of *homogenization* to define the macroscopic strain tensor ε at a point x of the macroscopic continuum as the volume average of its microscopic counterpart $\varepsilon_\mu := \nabla^s u_\mu$ over

the corresponding RVE:

$$\varepsilon := \frac{1}{V_\mu}\int_{\Omega_\mu} \nabla^s u_\mu = \frac{1}{V_\mu}\int_{\partial\Omega_\mu} u_\mu \otimes_s n \ , \tag{2.1}$$

where V_μ denotes the total volume of the RVE, u_μ is the microscopic displacement field of the RVE, n is the outward unit normal to the boundary $\partial\Omega_\mu$, ∇^s is the symmetric gradient operator and $\otimes_s$ denotes the symmetric tensor product between vectors.

For the purposes of the present paper, we shall consider RVEs whose domain consists of a matrix Ω_μ^m, containing inclusions of different materials occupying a domain Ω_μ^i (see Fig. 1). Further, we shall assume the matrix and the inclusions to be modelled as isotropic homogeneous materials. Hence, the microscopic stress tensor field $\sigma_\mu(\xi)$ satisfies

$$\sigma_\mu(\xi) = \mathbb{C}_\mu \nabla^s \xi \ , \tag{2.2}$$

where $\mathbb{C}_\mu$ is the fourth-order isotropic elasticity tensor field of the RVE:

$$\mathbb{C}_\mu := \frac{E_\mu}{1-\nu_\mu^2}\left[(1-\nu_\mu)\,\mathbb{I} + \nu_\mu\,(\mathrm{I}\otimes\mathrm{I})\right] \ , \tag{2.3}$$

with I and $\mathbb{I}$ denoting, respectively, the second- and fourth-order identity tensors and E_μ and ν_μ the Young's modulus and Poisson ratio fields of the RVE, given by

$$E_\mu(y) := \left\{ \begin{array}{ccc} E_\mu^m & \text{if} & y \in \Omega_\mu^m \\ E_\mu^i & \text{if} & y \in \Omega_\mu^i \end{array} \right. \quad \text{and} \quad \nu_\mu(y) := \left\{ \begin{array}{ccc} \nu_\mu^m & \text{if} & y \in \Omega_\mu^m \\ \nu_\mu^i & \text{if} & y \in \Omega_\mu^i \end{array} \right. \ . \tag{2.4}$$

If the RVE has more than one inclusion, the parameters E_μ^i and ν_μ^i are considered piecewise constant over Ω_μ^i.

Without loss of generality, u_μ may be decomposed into a sum

$$u_\mu\,(y) = u + \overline{u}_\mu\,(y) + \widetilde{u}_\mu\,(y) \ , \tag{2.5}$$

of a constant (rigid) RVE displacement coinciding with the macroscopic displacement $u(x)$, a linear field $\overline{u}_\mu\,(y) := \varepsilon y$, and a displacement fluctuation field $\widetilde{u}_\mu(y)$. This, together with (2.1), (2.2) and the Hill-Mandel Principle of Macro-Homogeneity [14, 15] leads to the *RVE mechanical equilibrium problem* which consists of finding, for a given macroscopic strain ε, an admissible microscopic displacement fluctuation field $\widetilde{u}_\mu \in \mathcal{U}_\mu$, such that

$$\int_{\Omega_\mu} \sigma_\mu(\overline{u}_\mu)\cdot\nabla^s\eta + \int_{\Omega_\mu} \sigma_\mu(\widetilde{u}_\mu)\cdot\nabla^s\eta = 0 \quad \forall \eta \in \mathcal{U}_\mu \ , \tag{2.6}$$

where

$$\sigma_\mu(\overline{u}_\mu) = \mathbb{C}_\mu\nabla^s\overline{u}_\mu; \qquad \sigma_\mu(\widetilde{u}_\mu) = \mathbb{C}_\mu\nabla^s\widetilde{u}_\mu, \tag{2.7}$$

and the (yet to be defined) space $\mathcal{U}_\mu$ of admissible displacement fluctuations (and virtual kinematically admissible displacements) fields of the RVE is a subspace of $\widetilde{\mathcal{U}}_\mu$ – the minimally constrained space of kinematically displacements of the RVE compatible with (2.1):

$$\mathcal{U}_\mu \subset \widetilde{\mathcal{U}}_\mu := \left\{ v \in [H^1(\Omega_\mu)]^2 : \int_{\Omega_\mu} v = 0, \int_{\partial\Omega_\mu} v \otimes_s n = 0 \right\}. \tag{2.8}$$

Once the problem (2.6) has been solved, the macroscopic stress tensor σ is obtained as the volume average of the microscopic stress field $\sigma_\mu(u_\mu) = \sigma_\mu(\overline{u}_\mu) + \sigma_\mu(\widetilde{u}_\mu)$ over the RVE, i.e.,

$$\sigma = \frac{1}{V_\mu}\int_{\Omega_\mu} \sigma_\mu(u_\mu) \ . \tag{2.9}$$

The complete characterization of the multi-scale constitutive model is obtained by defining the subspace $\mathcal{U}_\mu \subset \widetilde{\mathcal{U}}_\mu$ of kinematically admissible displacement fluctuations. In general, different choices produce different macroscopic responses for the same RVE. For example, the choice $\mathcal{U}_\mu = \widetilde{\mathcal{U}}_\mu$ results in a lower bound for the homogenised elastic properties. In the present paper, the analysis wil be focussed on media with periodic microstructure. In this case, the geometry of the RVE cannot be arbitrary and must represent a cell whose periodic repetition generates the macroscopic continuum. In addition, the displacement fluctuations must satisfy periodicity on the boundary of the RVE. Accordingly, we have

$$\mathcal{U}_\mu := \left\{ \widetilde{u}_\mu \in \widetilde{\mathcal{U}}_\mu : \widetilde{u}_\mu(y^+) = \widetilde{u}_\mu(y^-)\ \forall (y^+, y^-) \in P \right\}, \tag{2.10}$$

where P is the set of pairs of points, defined by a one-to-one periodicity correspondence, lying on opposing sides of the RVE boundary.

2.1. **The homogenized elasticity tensor.** Crucial to the developments presented in Section 3, is the closed form of the homogenized elasticity tensor $\mathbb{C}$ for the multi-scale model defined in the above. This can be obtained by means of the methodology suggested in [34], which is based on rewriting problem (2.6) as a superposition of linear problems associated with the individual Cartesian components of the macroscopic strain tensor. The components of the homogenized elasticity tensor $\mathbb{C}$, in the orthonormal basis $\{e_i\}$ of the Euclidean space, can be written as

$$(\mathbb{C})_{ijkl} = \frac{1}{V_\mu} \int_{\Omega_\mu} (\sigma_\mu(u_{\mu_{kl}}))_{ij} \ . \tag{2.11}$$

By virtue of (2.6), the canonical microscopic displacement field $u_{\mu_{kl}}$ associated with the tensors $\varepsilon_{kl} = e_k \otimes e_l$ is the solution of the equilibrium equation

$$\int_{\Omega_\mu} \sigma_\mu(u_{\mu_{kl}}) \cdot \nabla^s \eta = 0 \quad \forall \eta \in \mathcal{U}_\mu \ . \tag{2.12}$$

Note that, in view of (2.5), we have

$$u_{\mu_{kl}} - u - (e_k \otimes e_l) y = \widetilde{u}_{\mu_{kl}} \in \mathcal{U}_\mu \, , \tag{2.13}$$

so that problem (2.12) is equivalent to finding the field $\widetilde{u}_{\mu_{kl}} \in \mathcal{U}_\mu$ such that

$$\int_{\Omega_\mu} \sigma_\mu(\widetilde{u}_{\mu_{kl}}) \cdot \nabla^s \eta + \int_{\Omega_\mu} \mathbb{C}_\mu (e_k \otimes_s e_l) \cdot \nabla^s \eta = 0 \quad \forall \eta \in \mathcal{U}_\mu \ . \tag{2.14}$$

3. The topological sensitivity of the homogenized elasticity tensor

A closed formula for the sensitivity of the homogenized elasticity tensor of (2.11) to the nucleation of a circular inclusion within the RVE is presented in this section. The presented formula is central to the algorithm for microstructural synthesis/optimization proposed and applied in Sections 4 and 5 and relies on the concepts of *topological asymptotic expansion* and *topological derivative*. These relatively new mathematical concepts have been originally introduced by Sokołowski and Zochowski [46]. They extend the conventional notion of differentiability and provide the correct mathematical framework for the treatment of inherently singular topological domain changes such as those produced by the introduction of an inclusion, as considered in the present context.

3.1. **Topological asymptotic expansion. Preliminary concepts.** Let ϕ be a shape functional whose value depends on a given domain the topology of which is parametrized by a non-negative scalar ρ. A nil value of ρ defines what we refer to as the original (or unperturbed) domain, so that $\phi(0)$ is the value taken by the shape functional for such a domain. Any other value $\rho > 0$ defines a domain that differs from the original one by a topological perturbation of size ρ. Let us assume that ϕ has sufficient regularity so that the following expansion is possible

$$\phi(\rho) = \phi(0) + f(\rho) D_T \phi + o(f(\rho)) \, , \tag{3.1}$$

where $\phi(\rho)$ denotes the value of the functional for the topologically perturbed domain, $f(\rho)$ is a non-negative function such that $f(\rho) \to 0$ when $\rho \to 0$ and $o(f(\rho))$ contains all terms of higher order in $f(\rho)$. Expression (3.1) is referred to as the *topological asymptotic expansion* of the functional ϕ and the term $D_T\phi$ of (3.1) is named the *topological derivative* of ϕ at the unperturbed domain.

3.2. **Topological derivative of the homogenized elasticity tensor.** To apply the concepts of topological asymptotic expansion and topological derivative in the present context of multi-scale linear elasticity models, we begin by defining the so-called original domain as a given generic RVE of the type described in Section 2. The topological perturbation of the original domain Ω_μ consists of the nucleation of a small inclusion of radius ρ denoted by $\mathcal{I}_\rho$. Formally, the perturbed RVE domain Ω_{μ_ρ} is obtained by first introducing a circular hole $\mathcal{H}_\rho$ of radius ρ centred at an arbitrary point $\widehat{y} \in \Omega_\mu$ and then replacing the region of the hole by a circular inclusion $\mathcal{I}_\rho$ of different material properties. That is, the perturbed domain is defined as $\Omega_{\mu_\rho} = \left(\Omega_\mu \backslash \overline{\mathcal{H}_\rho}\right) \cup \mathcal{I}_\rho$ (refer to Fig. 2).

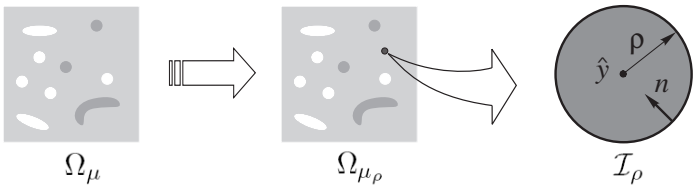

FIGURE 2. Topological perturbation at the microscopic level.

We shall assume that the microscopic elasticity tensor field of the perturbed RVE is given by

$$\mathbb{C}_\mu^\rho := \begin{cases} \mathbb{C}_\mu & \text{in} \quad \Omega_\mu \setminus \overline{\mathcal{H}_\rho} \\ \gamma \mathbb{C}_\mu & \text{in} \quad \mathcal{I}_\rho, \end{cases} \tag{3.2}$$

where the parameter $\gamma \geq 0$ defines the contrast between the elasticity tensor of the region of the original domain Ω_μ where the inclusion was inserted and the elasticity tensor of the inclusion material. We note that this type of perturbation corresponds to a change only in Young's modulus of the phases. Now, with this definition at hand, we denote the effective microscopic stress in the domain Ω_{μ_ρ} by

$$\sigma_\mu^\rho(\xi) = \mathbb{C}_\mu^\rho \nabla^s \xi = \begin{cases} \sigma_\mu(\xi) & \text{in} \quad \Omega_\mu \setminus \overline{\mathcal{H}_\rho} \\ \gamma \sigma_\mu(\xi) & \text{in} \quad \mathcal{I}_\rho. \end{cases} \tag{3.3}$$

From the above expression and (2.11) the components of the macroscopic elasticity tensor corresponding to Ω_{μ_ρ} can be obtained as

$$(\mathbb{C}^\rho)_{ijkl} = \frac{1}{V_\mu} \int_{\Omega_\mu} (\sigma_\mu^\rho(u_{\mu_{kl}}^\rho))_{ij} \, , \tag{3.4}$$

where the canonical microscopic displacement field $u_{\mu_{kl}}^\rho$ associated to the topologically perturbed domain satisfies

$$\int_{\Omega_\mu} \sigma_\mu^\rho(u_{\mu_{kl}}^\rho) \cdot \nabla^s \eta = 0 \quad \forall \eta \in \mathcal{U}_\mu \tag{3.5}$$

and, analogously to (2.13), we have

$$u_{\mu_{kl}}^\rho - u - (e_k \otimes e_l) y = \widetilde{u}_{\mu_{kl}}^\rho \in \mathcal{U}_\mu \, , \tag{3.6}$$

where $\widetilde{u}_{\mu_{kl}}^\rho$ is the displacement fluctuation field associated to the perturbed domain Ω_{μ_ρ} and to the tensor $e_k \otimes e_l$.

With the above definitions at hand, we may now specialize (3.1) by identifying the shape functional ϕ with the homogenized elasticity tensor. The resulting topological asymptotic expansion of $\mathbb{C}$ reads

$$\mathbb{C}^\rho = \mathbb{C} + f(\rho) \, D_T \mathbb{C} + o(f(\rho)) \, . \tag{3.7}$$

This expansion is indeed possible and its derivation for two-dimensional problems is addressed in the appendix. The function f in this case is found to be

$$f(\rho) = \frac{\pi \rho^2}{V_\mu} \, , \tag{3.8}$$

i.e. it represents the volume fraction of the inserted inclusion. The *topological derivative of the homogenized elasticity tensor* at the unperturbed RVE domain, denoted $D_T \mathbb{C}$, is a fourth-order tensor field over Ω_μ that provides a rigorous first order approximation (in ρ) to the change in $\mathbb{C}$ resulting from the insertion of a circular inclusion of radius ρ within the RVE. Its *closed form* expression in Cartesian components reads

$$(D_T \mathbb{C})_{ijkl} = \mathbb{H}_\gamma \sigma_\mu(u_{\mu_{ij}}) \cdot \sigma_\mu(u_{\mu_{kl}}) \, , \tag{3.9}$$

where the fields $u_{\mu_{ij}}$ are the solutions to (2.12) for the *unperturbed* RVE domain and the fourth-order tensor $\mathbb{H}_\gamma$ is defined as

$$\mathbb{H}_\gamma := -\frac{1}{E_\mu} \left(\frac{1-\gamma}{1+\alpha\gamma} \right) \left[4\mathbb{I} - \frac{1-\gamma(\alpha-2\beta)}{1+\beta\gamma} \, (\mathrm{I} \otimes \mathrm{I}) \right] \, . \tag{3.10}$$

with

$$\alpha = \frac{1+\nu_\mu}{1-\nu_\mu} \, , \qquad \beta = \frac{3-\nu_\mu}{1+\nu_\mu} \, . \tag{3.11}$$

Remark 1. *The above analytical formula for the topological derivative field is particularly suitable for implementation within finite element-based numerical frameworks. Its computation in this context (considered in Sections 4 and 5) is* extremely simple*: Once the finite element approximations to the vector fields $u_{\mu_{ij}}$ are obtained as solutions of the discretized version of problem (2.12) for the* original *domain, the corresponding discretized version of the fourth-order tensor field $D_T\mathbb{C}$ can be promptly calculated according to (3.9).*

Remark 2. *Expression (3.9) allows the* exact *derivative of any differentiable function of $\mathbb{C}$ with respect to the volume fraction of inclusion to be calculated through the direct application of the conventional rules of differential calculus. That is, any such a function $h(\mathbb{C})$ has exact topological derivative*

$$D_T h = \langle Dh(\mathbb{C}), D_T\mathbb{C} \rangle \,, \tag{3.12}$$

with the brackets $\langle \cdot, \cdot \rangle$ denoting the appropriate product between the two terms – the derivative of h with respect to $\mathbb{C}$ and the topological derivative of $\mathbb{C}$. Note, for example, that properties of interest such as the homogenized Young's, shear and bulk moduli as well as the Poisson ratio are all regular functions of $\mathbb{C}$. This observation together with Remark 1 point strongly to the suitability of the use of (3.7) in a finite element-based framework for the synthesis and optimization of elastic micro-structures based on the minimization/maximization of cost functions defined in terms of homogenized properties. This is the main aim of the present paper and will be pursued in Sections 4 and 5.

Remark 3. *The tensor $\mathbb{H}_\gamma$ has an explicit dependency on the phase contrast parameter γ. In the limiting case with $\gamma \to \infty$, corresponding to the insertion of a* rigid inclusion*, we have*

$$\mathbb{H}_\infty = \frac{1}{E_\mu \alpha}\left[4\mathbb{I} + \frac{\alpha - 2\beta}{\beta}(\mathrm{I}\otimes\mathrm{I})\right]. \tag{3.13}$$

The limit $\gamma \to 0$, on the other hand, corresponds to the insertion of a hole *in the RVE. In this case we have*

$$\mathbb{H}_0 = -\frac{1}{E_\mu}[4\mathbb{I} - (\mathrm{I}\otimes\mathrm{I})]. \tag{3.14}$$

This last expression coincides with the result derived in [22].

4. A topological derivative-based micro-structure design algorithm

In this section we propose a microstucture topology design algorithm based on the topological asymptotic expansion (3.7) of the homogenized elasticity tensor. The RVE domain here represents a bi-material microstructure whose constituents properties are defined by a given elasticity tensor $\mathbb{C}^*$ and phase contrast γ^* so that, as in (3.2), we have

$$\mathbb{C}_\mu(y) = \begin{cases} \mathbb{C}^*_\mu & \forall y \in \Omega^1_\mu \\ \gamma^*\,\mathbb{C}^*_\mu & \forall y \in \Omega^2_\mu, \end{cases} \tag{4.1}$$

where Ω^1_μ and Ω^2_μ denote the domains occupied by materials 1 and 2, respectively. The sought topology of the RVE is the solution of the general optimization problem stated as

$$\underset{\Omega^1_\mu \subset \Omega_\mu}{\text{Minimize}}\, J(\Omega^1_\mu) = h(\mathbb{C}) + \lambda \frac{|\Omega^1_\mu|}{V_\mu} \,, \tag{4.2}$$

where the cost function J is a scalar-valued functional of the domain Ω^1_μ, h is a generic (yet to be defined) function of the homogenized elasticity tensor $\mathbb{C}$ and λ is a fixed Lagrange multiplier which imposes a constraint on the volume ratio of material 1 (with volume denoted $|\Omega^1_\mu|$).

It should be stressed that the design variable in problem (4.2) is the topology of the domain Ω^1_μ. Hence, the use of the *exact* topological sensitivity information provided by the topological derivative (3.9) emerges as a natural alternative in the development of a numerical optimization algorithm to tackle the problem. In this context, by taking into account the comments made in Remark 2, we see that the topological derivative of the cost function, i.e. the exact derivative of J with respect to the volume fraction of an inclusion of radius ρ centred at an arbitrary point $y \in \Omega_\mu$ is given by the simple general formula

$$D_T J(y) = \langle Dh(\mathbb{C}), D_T\mathbb{C}(y) \rangle + \lambda \,. \tag{4.3}$$

At this point, it is worth remarking that the *inclusion* referred to above is assumed to be made of material 2 at points $y \in \Omega^1_\mu$ and of material 1 at points $y \in \Omega^2_\mu$ so that (4.3) always measures the sensitivity of J

when materials 1 and 2 are interchanged within the RVE. This allows the algorithm (described below) to replace, for example, material 1 with material 2 and then replace material 2 back with material 1 and so on at any given region of the RVE. Following this observation, the computation of (4.3) is carried out using the expressions (3.9–3.11) with $\gamma = \gamma^*$ if $y \in \Omega_\mu^1$ and $\gamma = 1/\gamma^*$ if $y \in \Omega_\mu^2$.

Having made the above considerations, the topological derivative-based optimization algorithm devised in [4] stands out as a particularly well-suited choice to solve problem (4.2). The procedure relies on a level-set domain representation [40] and the approximation of the topological optimality conditions by a fixed point iteration. In particular, the algorithm displays a marked ability to produce general topological domain changes uncommon to other methodologies based on a level-set representation and has been successfully applied in [4] to topology optimization in the context of two-dimensional elasticity and flow through porous media. For completeness, the algorithm is outlined in the following. For further details we refer to [4].

With the adoption of a level-set domain representation, the current material 1 domain, Ω_μ^1, is characterized by a function $\psi \in L^2(\Omega_\mu)$ such that

$$\Omega_\mu^1 = \{y \in \Omega_\mu, \psi(y) < 0\}, \tag{4.4}$$

whereas the material 2 domain is defined by

$$\Omega_\mu^2 = \{y \in \Omega_\mu, \psi(y) > 0\}. \tag{4.5}$$

Now, let us consider the topological derivative field $D_T J$ of formula (4.3). According to [4], an obvious sufficient condition of local optimality of problem (4.2) for the class of perturbations consisting of circular inclusions is

$$D_T J(y) > 0 \quad \forall y \in \Omega_\mu. \tag{4.6}$$

To devise a level-set-based algorithm whose aim is to produce a topology that satisfies (4.6) it is convenient to define the function

$$g(y) = \begin{cases} -D_T J(\Omega_\mu^1)(y) & \text{if} \quad y \in \Omega_\mu^1 \\ D_T J(\Omega_\mu^1)(y) & \text{if} \quad y \in \Omega_\mu^2. \end{cases} \tag{4.7}$$

With the above definition and (4.4,4.5) it can be easily established that the sufficient condition (4.6) is satisfied if the following equivalence relation between g and the level-set function ψ holds

$$\exists\, \tau > 0 \quad \text{s.t.} \quad g = \tau\, \psi, \tag{4.8}$$

or, equivalently,

$$\theta := \arccos\left[\frac{\langle g, \psi\rangle}{\|g\|_{L^2}\, \|\psi\|_{L^2}}\right] = 0, \tag{4.9}$$

where θ is the angle between the vectors g and ψ in $L^2(\Omega_\mu)$.

Starting from a given level-set function $\psi_0 \in L^2(\Omega_\mu)$ which defines the chosen initial guess for the optimum topology, the algorithm proposed in [4] produces a sequence $(\psi_i)_{i\in\mathbb{N}}$ of level-set functions (corresponding to a sequence of RVE topologies) that provides successive approximations to the sufficient condition for optimality (4.8). The sequence satisfies

$$\begin{aligned} &\psi_0 \in L^2(\Omega_\mu)\ , \\ &\psi_{n+1} \in \mathrm{co}(\psi_n, g_n) \qquad \forall n \in \mathbb{N}, \end{aligned} \tag{4.10}$$

where $\mathrm{co}(\psi_n, g_n)$ is the convex hull of $\{\psi_n, g_n\}$. In the actual algorithm the initial guess ψ_0 is normalized. With $\mathcal{S}$ denoting the unit sphere in $L^2(\Omega_\mu)$, the algorithm is explicitly given by

$$\begin{aligned} &\psi_0 \in \mathcal{S}\ , \\ &\psi_{n+1} = \frac{1}{\sin\theta_n}\left[\sin((1-\kappa_n)\theta_n)\psi_n + \sin(\kappa_n\theta_n)\tfrac{g_n}{\|g_n\|_{L^2}}\right] \qquad \forall n \in \mathbb{N}, \end{aligned} \tag{4.11}$$

where $\kappa_n \in [0,1]$ is a step size determined by a line-search in order to decrease the value of the cost functional J and, by construction of $(4.11)_2$, we have that $\psi_{n+1} \in \mathcal{S}\ \forall n \in \mathbb{N}$. The iterative process is stopped when for some iteration the obtained decrease in J is smaller than a given numerical tolerance. If, at this stage, the optimality condition (4.8,4.9) is not satisfied to the desired degree of accuracy, i.e. if

$$\theta_{n+1} > \epsilon_\theta, \tag{4.12}$$

where ϵ_θ is a pre-specified convergence tolerance, then a uniform mesh refinement of the RVE is carried out and the procedure is continued.

4.1. **Finite element implementation.** In the computation of $\mathbb{C}$ according to (2.11–2.14), we obtain the fields $\tilde{u}_{kl}$ by a finite element discretization of (2.14). In particular, the periodicity of the boundary displacement fluctuations is enforced by a direct approach according to the implementation described in [21]. In the computation of $D_T J$ with (4.3), a finite element approximation to the topological gradient field $D_T\mathbb{C}$ is used. The approximation is obtained by first using the finite element solutions $u_{\mu_{kl}}$ in (3.9) and then smoothing each component field $(D_T\mathbb{C})_{ijkl}$ in a standard fashion. That is, the final discretised version of the tensor field $D_T\mathbb{C}$ is generated by the finite element shape functions with smoothed nodal values of $(D_T\mathbb{C})_{ijkl}$. The level-set functions ψ_n are generated by the same shape functions used in the finite element approximation of problem (2.14). In this context, the following approximation is used for the bi-material micro-structure. The material property associated with Ω_μ^1 (Ω_μ^2) is assigned to the nodes with negative (positive) level-set function ψ_n. The material property within the element is obtained by a standard interpolation using the element shape functions. Obviously, the resolution of the RVE domain topology depends directly on the fineness of the adopted mesh.

Remark 4. *The present algorithm is of simple implementation. The updated level-set function ψ_{n+1} obtained at iteration $n+1$ according to (4.11) is only a linear combination between the known function ψ_n and the corresponding function g_n, which depends on the topological gradient $D_T J$ for the known topology of iteration n. The computation of these quantities is straightforward. Note, in particular, that* no artificial algorithmic parameters or post-processing strategies *are required throughout the iterations. This is in sharp contrast with existing microstructural optimization strategies and follows as a natural consequence of the use of the concept of topological derivative. This concept provides the correct mathematical framework for the rigorous treatment of topology changes of the type present in microstructural optimization problems.*

5. Numerical examples

The application of the above optimization algorithm to the synthesis of microstructures is illustrated in this section by means of a series of numerical examples.

Following the usual convention we write the homogenized two-dimensional elasticity tensor $\mathbb{C}$ in matrix form:

$$C = \begin{pmatrix} (\mathbb{C})_{1111} & (\mathbb{C})_{1122} & (\mathbb{C})_{1112} \\ (\mathbb{C})_{1122} & (\mathbb{C})_{2222} & (\mathbb{C})_{2212} \\ (\mathbb{C})_{1112} & (\mathbb{C})_{2212} & (\mathbb{C})_{1212} \end{pmatrix}. \tag{5.1}$$

For the case orthotropic symmetry, the effective material properties – the Young's, bulk and shear moduli as well as the Poisson's ratios – are related explicitly to the components of the compliance tensor $\mathbb{C}^{-1}$, whose matrix representation reads

$$C^{-1} = \begin{pmatrix} (\mathbb{C}^{-1})_{1111} & (\mathbb{C}^{-1})_{1122} & 0 \\ (\mathbb{C}^{-1})_{1122} & (\mathbb{C}^{-1})_{2222} & 0 \\ 0 & 0 & (\mathbb{C}^{-1})_{1212} \end{pmatrix} = \begin{pmatrix} \frac{1}{E_1} & -\frac{\nu_{12}}{E_1} & 0 \\ -\frac{\nu_{21}}{E_2} & \frac{1}{E_2} & 0 \\ 0 & 0 & \frac{1}{G} \end{pmatrix}, \tag{5.2}$$

where E_1, E_2 are the effective Young's moduli along the orthotropy directions e_1 and e_2, respectively, G is the effective in-plane shear modulus and ν_{12} and ν_{21} are the effective Poisson's ratios satisfying

$$\frac{\nu_{21}}{E_2} = \frac{\nu_{12}}{E_1}. \tag{5.3}$$

In the examples that follow we shall use the algorithm of Section 4 to sinthesize microstructures with optimized effective properties. To this end, it is convenient to define the following types of functions $h(\mathbb{C})$:

- The first type of functions is defined as

$$h(\mathbb{C}) = \mathbb{C}^{-1}\varphi_1 \cdot \varphi_2 \,, \tag{5.4}$$

  where φ_1 and φ_2 are second order tensors to be defined later. The topological derivative of the associated cost function J of (4.2) in this case reads

$$D_T J = -(\mathbb{C}^{-1}(D_T\mathbb{C})\mathbb{C}^{-1})\varphi_1 \cdot \varphi_2 + \lambda \,. \tag{5.5}$$

- The second type is defined as

$$h(\mathbb{C}) = \frac{\mathbb{C}^{-1}\varphi_1 \cdot \varphi_2}{\mathbb{C}^{-1}\varphi_1 \cdot \varphi_1} + \frac{\mathbb{C}^{-1}\varphi_2 \cdot \varphi_1}{\mathbb{C}^{-1}\varphi_2 \cdot \varphi_2} \,. \tag{5.6}$$

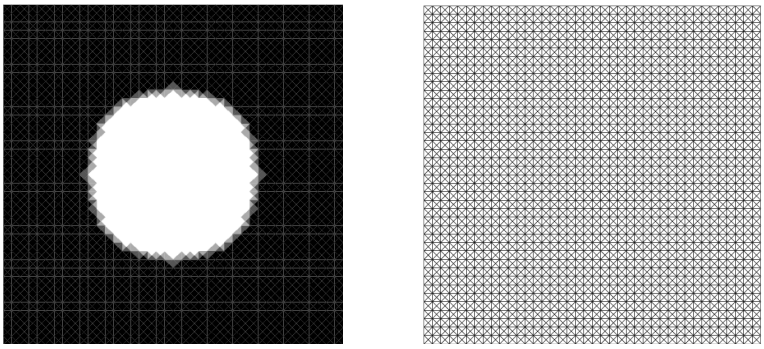

(a) (b)

FIGURE 3. Microstructural synthesis examples. (a) Initial guess for the optimum topology, and; (b) Initial finite element mesh adopted.

The corresponding topological derivative of J here is

$$D_T J = - \frac{(\mathbb{C}^{-1}(D_T\mathbb{C})\mathbb{C}^{-1})\varphi_1 \cdot [(\mathbb{C}^{-1}\varphi_1 \cdot \varphi_1)\varphi_2 - (\mathbb{C}^{-1}\varphi_1 \cdot \varphi_2)\varphi_1]}{(\mathbb{C}^{-1}\varphi_1 \cdot \varphi_1)^2} - \frac{(\mathbb{C}^{-1}(D_T\mathbb{C})\mathbb{C}^{-1})\varphi_2 \cdot [(\mathbb{C}^{-1}\varphi_2 \cdot \varphi_2)\varphi_1 - (\mathbb{C}^{-1}\varphi_2 \cdot \varphi_1)\varphi_2]}{(\mathbb{C}^{-1}\varphi_2 \cdot \varphi_2)^2} + \lambda \,. \tag{5.7}$$

In all examples the RVE domain is taken as the the unit square $\Omega_\mu = (0,1) \times (0,1)$. The Young's modulus and the Poisson ratio of materials 1 and 2 are, respectively, $E^1_\mu = 1$, $E^2_\mu = 0.01$ and $\nu^1_\mu = \nu^2_\mu = 0.3$. That is, we consider a phase contrast parameter $\gamma^* = 0.01$. The specified convergence tolerance for the angle θ is $\epsilon_\theta = 1^\circ$. We remark that our numerical experience shows that this choice provides a particularly stringent criterion producing solutions that satisfy the sufficient condition (4.8) for optimality very closely. The adopted initial guess for the optimum topology in all cases is defined by the level-set function

$$\psi_0 = \frac{1}{N}\left[\cos^2(\pi(x - x_0))\cos^2(\pi(y - y_0)) - 0.5\right] \,, \tag{5.8}$$

where N is the normalizing constant that ensures that $\|\psi\|_{L^2} = 1$. Unless otherwise stated, we choose $(x_0, y_0) = (0.5, 0.5)$. The topology of the RVE domain in this case is illustrated in fig. 3(a), where the dark- and light-coloured areas denote respectively materials 1 and 2. Also depicted in fig. 3 is the initial (regular) mesh discretizing the RVE. It consists of 6400 three-noded linear triangles and a total of 3281 nodes.

5.1. **Basic cases.** In this section we consider only functions $h(\mathbb{C})$ of the type (5.4). In each case the algorithm converges with the initial mesh to the prescribed accuracy of $\epsilon_\theta = 1^\circ$. Despite the good accuracy attained with the initial mesh alone, we perform one uniform mesh refinement step to further improve the accuracy of the results and the resolution of the optimized RVE topology. The final meshes have 25,600 elements and 12,961 nodes.

5.1.1. *Horizontal rigidity maximization.* This is a trivial case where we choose $\varphi_1 = \varphi_2 = e_1 \otimes e_1$, with e_1 denoting the unit vector in the horizontal direction. Then, the corresponding function $h(\mathbb{C})$ is given by

$$h(\mathbb{C}) := (\mathbb{C}^{-1})_{1111} = \frac{1}{E_1} \,. \tag{5.9}$$

Note that the minimization of $h(\mathbb{C})$ in this case corresponds to the maximization of the longitudinal Young's modulus E_1. In addition we choose $\lambda = 10$. The obtained optimized RVE topology is shown in fig. 4(a). The corresponding periodic microstructure is illustrated in fig. 4(b). The evolution of the cost function and angle θ throughout the iterations of $(4.11)_2$ are shown in fig. 5. Here the mesh refinement step has been performed at iteration 9, at which the residual angle θ is sufficiently small. Following the refinement, there is a small increase in θ (iteration 10), followed by a sharp decrease at iteration 11, at which final convergence is attained.

(a) (b)

FIGURE 4. Horizontal rigidity maximization: (a) Optimum RVE topology, and; (b) Periodic microstructure.

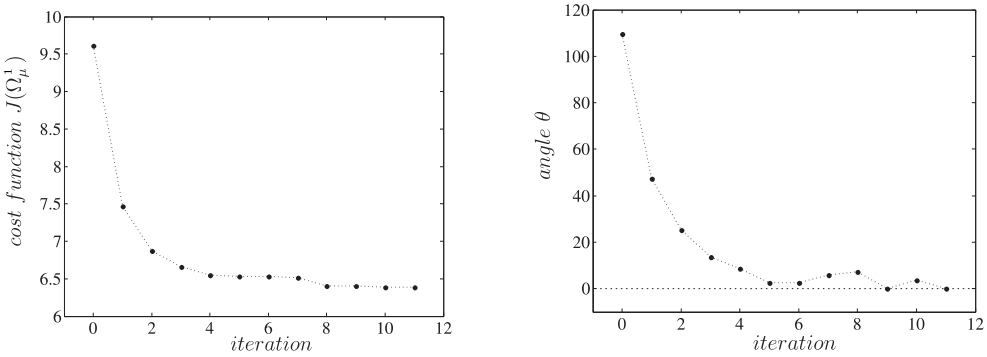

(a) (b)

FIGURE 5. Horizontal rigidity maximization. Convergence history: (a) Cost function, and; (b) Angle θ.

5.1.2. *Bulk modulus maximization.* In this case, we choose $\varphi_1 = \varphi_2 = e_1 \otimes e_1 + e_2 \otimes e_2$. The corresponding function $h(\mathbb{C})$ is

$$h(\mathbb{C}) := (\mathbb{C}^{-1})_{1111} + 2(\mathbb{C}^{-1})_{1122} + (\mathbb{C}^{-1})_{2222} = \frac{1}{E_1}(1 - \nu_{12}) + \frac{1}{E_2}(1 - \nu_{21}). \tag{5.10}$$

We choose $\lambda = 20$. The optimum RVE topology obtained is depicted in fig. 6 alongside an illustration of the corresponding periodic microstructure. The total number of iterations needed to reach the optimum topology in the presente case was 21 (including the interations after the mesh refinement step).

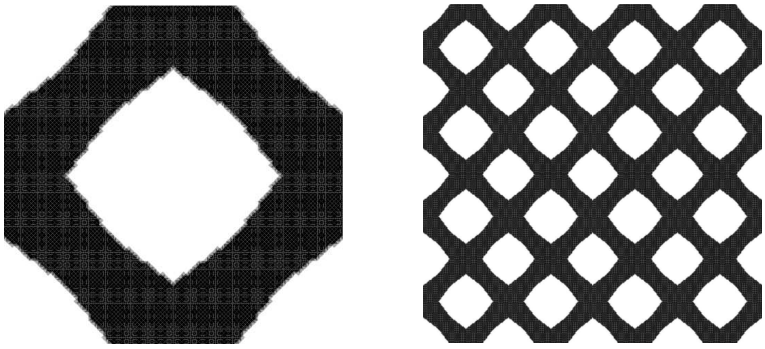

(a) (b)

FIGURE 7. Shear modulus maximization. (a) Optimized RVE, and; (b) Corresponding periodic microstructure.

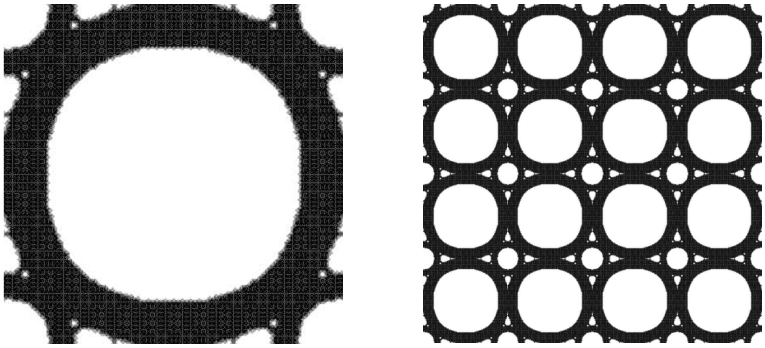

(a) (b)

FIGURE 6. Bulk modulus maximization. (a) Optimized RVE topology, and; (b) Corresponding periodic microstructure.

5.1.3. *Shear modulus maximization.* Here we take $\varphi_1 = \varphi_2 = e_1 \otimes e_2 + e_2 \otimes e_1$ so that $h(\mathbb{C})$ is simply

$$h(\mathbb{C}) = 4(\mathbb{C}^{-1})_{1212} \,. \tag{5.11}$$

The minimization of the present function h corresponds to the maximization of the effective shear modulus G. The Lagrange multiplier is chosen as $\lambda = 50$. The final optimized topology obtained is shown in fig. 7. A total of 10 interations were required to achieve convergence.

5.2. **Poisson's ratio optimization.** In this section we present four examples associated with the optimization of the Poisson's ratio. In the first two cases we consider functions $h(\mathbb{C})$ of the form (5.4) and, in the last two cases, functions of the type (5.6). In all four examples, we perform two steps of uniform mesh refinement during the optimization process. The final meshes contain a total of $102,400$ three-noded elements and $51,521$ nodes. The Lagrange multiplier is set to $\lambda = 0$ so that no constraints are imposed on the volume ratio of the phases.

5.2.1. *Minimization of a modified Poisson ratio.* In this first case, we set $\varphi_1 = e_1 \otimes e_1$ and $\varphi_2 = -e_2 \otimes e_2$ in (5.4). The corresponding function $h(\mathbb{C})$ is

$$h(\mathbb{C}) := -(\mathbb{C}^{-1})_{1122} = \frac{\nu_{12}}{E_1} = \frac{\nu_{21}}{E_2} \,. \tag{5.12}$$

The final topology, obtained here in 45 iterations, is shown in fig. 8. The corresponding homogenized elasticity tensor, in matrix representation, is found to be

$$C = \begin{pmatrix} 0.0825 & -0.0308 & 0 \\ -0.0308 & 0.0825 & 0 \\ 0 & 0 & 0.0105 \end{pmatrix}, \tag{5.13}$$

which yields a negative Poisson ratio, $\nu = -0.3740$.

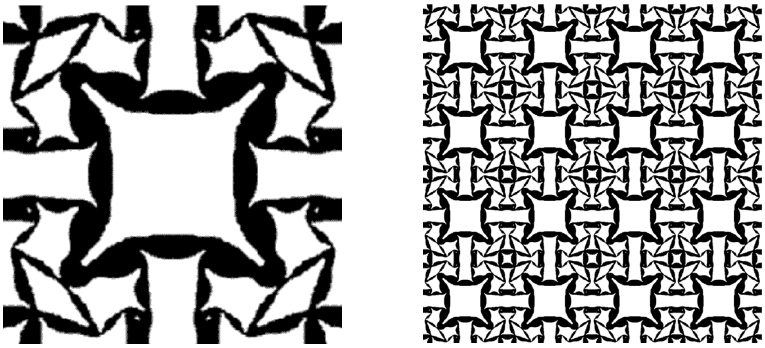

(a) (b)

FIGURE 8. Minimization of a modified Poisson ratio: (a) Optimized RVE, and; (b) Corresponding periodic microstructure.

5.2.2. *Maximization of a modified Poisson ratio.* Here we set $\varphi_1 = e_1 \otimes e_1$ and $\varphi_2 = e_2 \otimes e_2$ so that

$$h(\mathbb{C}) := (\mathbb{C}^{-1})_{1122} = -\frac{\nu_{12}}{E_1} = -\frac{\nu_{21}}{E_2}\,. \tag{5.14}$$

The final topology, obtained in 32 iterations is depicted in fig. 9(a) alogside the resulting periodic microstructure. The matrix form of the corresponding homogenized elasticity is

$$C = \begin{pmatrix} 0.0469 & 0.0368 & 0 \\ 0.0368 & 0.0469 & 0 \\ 0 & 0 & 0.0098 \end{pmatrix}, \tag{5.15}$$

with a resulting Poisson's ratio $\nu = 0.7847$.

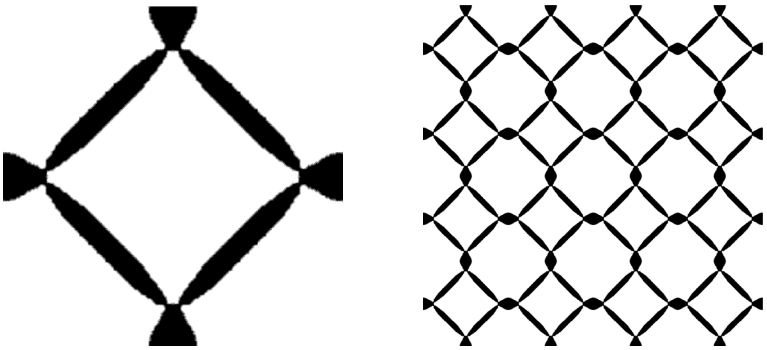

(a) (b)

FIGURE 9. Maximization of a modified Poisson's ratio: (a) Optimized RVE, and; (b) Corresponding periodic microstructure.

5.2.3. *Poisson's ratio minimization.* Here we use $\varphi_1 = e_1 \otimes e_1$ and $\varphi_2 = -e_2 \otimes e_2$ in (5.6). The resulting function $h(\mathbb{C})$ is

$$h(\mathbb{C}) := -\frac{(\mathbb{C}^{-1})_{1122}}{(\mathbb{C}^{-1})_{1111}} - \frac{(\mathbb{C}^{-1})_{1122}}{(\mathbb{C}^{-1})_{2222}} = \nu_{12} + \nu_{21}. \tag{5.16}$$

The obtained optimized topology is shown in fig. 10(a). The matrix representation of the corresponding $\mathbb{C}$ is

$$C = \begin{pmatrix} 0.1939 & -0.0669 & 0 \\ -0.0669 & 0.1939 & 0 \\ 0 & 0 & 0.0311 \end{pmatrix}, \tag{5.17}$$

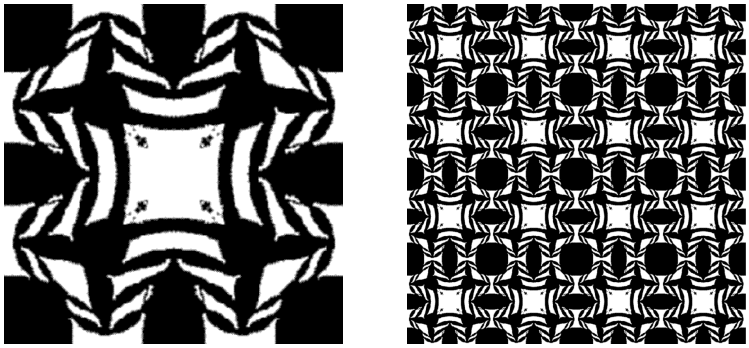

FIGURE 10. Minimization of the Poisson ratio.

which results in the negative Poisson ratio $\nu = -0.3452$. In this case, the algorithm does not converge well initially (the value of J stops decreasing significantly with $\theta \approx 7^o$). This is probably due to an ill-conditioning of the problem. However, by performing another step of uniform mesh refinement we obtain a better convergence with a final topology having $\theta < 5^o$ and a Poisson ratio $\nu = -0.4118$. The final resulting topology is depicted in fig. 11 together with the convergence history of the cost function $h(\mathbb{C})$. A total number of 73 iterations where required to achieve convergence with $\epsilon_\theta = 5°$.

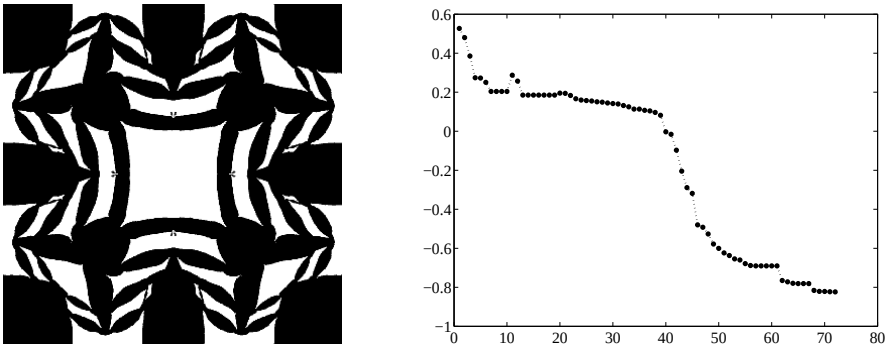

(a) (b)

FIGURE 11. Minimization of the Poisson ratio: (a) Final topology, and; (b) Convergence history of the cost function.

5.2.4. *Poisson ratio maximization.* In this last example we set $\varphi_1 = e_1 \otimes e_1$ and $\varphi_2 = e_2 \otimes e_2$ and the resultind function $h(\mathbb{C})$ is

$$h(\mathbb{C}) := \frac{(\mathbb{C}^{-1})_{1122}}{(\mathbb{C}^{-1})_{1111}} + \frac{(\mathbb{C}^{-1})_{1122}}{(\mathbb{C}^{-1})_{2222}} = -\nu_{12} - \nu_{21}. \tag{5.18}$$

The converged optimzed topology of the RVE, attained in 35 iterations, is shown in fig. 12(a). The associated homogenized elasticity tensor is given by

$$C = \begin{pmatrix} 0.1565 & 0.1363 & 0 \\ 0.1363 & 0.1565 & 0 \\ 0 & 0 & 0.1162 \end{pmatrix}, \tag{5.19}$$

which gives a Poisson's ratio $\nu = 0.8711$.

6. CONCLUSION

An algorithm for the topological design of periodic microstructures has been proposed. The algorithm relies crucially on an *exact* formula for the topological derivative of the homogenized elasticity tensor and a level-set domain representation. The homogenized elasticity tensor is estimated by a well-established multi-scale constitutive theory in which the macroscopic stress and strain tensors are volume averages of

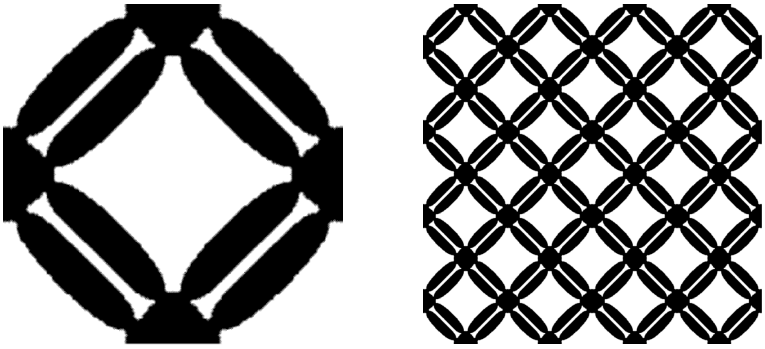

(a) (b)

FIGURE 12. Maximization of the Poisson ratio: (a) Optimized RVE topology, and; (b) Corresponding periodic microstructure.

their microscopic counterparts over a Representative Volume Element (RVE). Its analytical topological derivative is a fourth order tensor field over the RVE that provides a rigorous first order approximation (in the volume fraction of inclusion) to the change in the homogenozed elasticity tensor resulting from the insertion of a circular inclusion of a given phase contrast parameter. The proposed algorithm was successfully and efficiently used in several numerical examples of optimum topology design of bi-material periodic microstructures. We remark that the algorithm is of simple implementation and, in sharp contrast to existing microstructural optimization methods, does not require the use of artificial algorithmic parameters or strategies. This is only a natural consequence of the use of the concept of topological derivative, which provides the correct mathematical framework to treat problems involving singular changes of topology such as those present in microstructural optimization problems. The application of the proposed methodology to other types of multi-scale models is currently in progress and will be reported in forthcoming publications.

ACKNOWLEDGEMENTS

This research was partly supported by The Royal Society (International Joint Project no. JP080066). S.M. Giusti was supported by the Brazilian Research, CNPq (grant no. 382485/2009-2). This support is gratefully acknowledged.

REFERENCES

[1] G. Allaire, F. de Gournay, F. Jouve, and A. Toader. Structural optimization using topological and shape sensitivity via a level set method. *Control Cybern.*, 34(1):59–80, 2005.
[2] R.F. Almgreen. An isotropic three-dimensional structure with Poisson's ratio -1. *J. Elast.*, 15(4):427–430, 1985.
[3] S. Amstutz. Sensitivity analysis with respect to a local perturbation of the material property. *Asymptot. Anal.*, 49(1-2):87–108, 2006.
[4] S. Amstutz and H. Andrä. A new algorithm for topology optimization using a level-set method. *J. Comput. Phys.*, 216(2):573–588, 2006.
[5] S. Amstutz, I. Horchani, and M. Masmoudi. Crack detection by the topological gradient method. *Control Cybern.*, 34(1):81–101, 2005.
[6] J.L. Auriault. Effective macroscopic description for heat conduction in periodic composites. *Int. J. Heat Mass Transf.*, 26(6):861–869, 1983.
[7] J.L. Auriault and P. Royer. Double conductivity media: a comparison between phenomenological and homogenization approaches. *Int. J. Heat Mass Transf.*, 36(10):2613–2621, 1993.
[8] D. Auroux, M. Masmoudi, and L. Belaid. Image restoration and classification by topological asymptotic expansion. In *Variational formulations in mechanics: theory and applications*, E. Taroco, E.A. de Souza Neto and A.A. Novotny (eds.), CIMNE, Barcelona, Spain, 2007.
[9] T. Belytschko, S.P. Xiao and C. Parimi. Topology optimization with implicit functions and regularization. *Int. J. Num. Meth. Engng.*, 57:1177–1196, 2003.
[10] M.P. Bendsøe and N. Kikuchi. Generating optimal topologies in structural design using an homogenization method. *Comput. Methods Appl. Mech. Eng.*, 71(2):197–224, 1988.
[11] A. Bensoussan, J.L. Lions, and G. Papanicolau. *Asymptotic analysis for periodic microstructures*. North Holland, Amsterdam, 1978.

[12] J. Céa, S. Garreau, Ph. Guillaume, and M. Masmoudi. The shape and topological optimizations connection. *Comput. Methods Appl. Mech. Eng.*, 188(4):713–726, 2000.

[13] D. J. Celentano, P. M. Dardati, L. A. Godoy, and R. E. Boeri. Computational simulation of microstructure evolution during solidification of ductile cast iron. *Int. J. Cast Met. Res.*, 21(6):416–426, 2008.

[14] E.A. de Souza Neto and R.A. Feijóo. Variational foundations of multi-scale constitutive models of solid: small and large strain kinematical formulation. Technical Report No 16/2006, Laboratório Nacional de Computação Científica LNCC/MCT, Petrópolis, Brazil, 2006.

[15] E.A. de Souza Neto and R.A. Feijóo. Axiomatic variational foundations of multi-scale solid constitutive models: kinematical formulation. In *Advanced computational materials modelling: From classical to multi-scale techniques*, M. Vaz Jr., E.A. de Souza Neto and P. Muñoz-Rojas (eds.), Wiley, Chichester, 2010 (to appear).

[16] H.A. Eschenauer, V.V. Kobelev, and A. Schumacher. Bubble method for topology and shape optmization of structures. *Struct. Optim.*, 8(1):42–51, 1994.

[17] H.A. Eschenauer and N. Olhoff. Topology optmization of continuum structures: a review. *Appl. Mech. Rev.*, 54(4):331–390, 2001.

[18] G.R. Feijóo. A new method in inverse scattering based on the topological derivative. *Inverse Probl.*, 20(6):1819–1840, 2004.

[19] S. Garreau, Ph. Guillaume, and M. Masmoudi. The topological asymptotic for pde systems: the elasticity case. *SIAM J. Control Optim.*, 39(6):1756–1778, 2001.

[20] P. Germain, Q.S. Nguyen, and P. Suquet. Continuum thermodynamics. *J. Appl. Mech., Trans. ASME*, 50(4):1010–1020, 1983.

[21] S.M. Giusti, P.J. Blanco, E.A. de Souza Neto, and R.A. Feijóo. An assessment of the Gurson yield criterion by a computational multi-scale approach. *Eng. Comput.*, 26(3):281–301, 2009.

[22] S.M. Giusti, A.A. Novotny, E.A. de Souza Neto, and R.A. Feijóo. Sensitivity of the macroscopic elasticity tensor to topological microstructural changes. *J. Mech. Phys. Solids*, 57(3):555–570, 2009.

[23] S.M. Giusti, A.A. Novotny and E.A. de Souza Neto. Sensitivity of the macroscopic response of elastic microstructures to the insertion of inclusions. *Proc. Roy. Soc. Lond. A*, 2009 (accepted for publication).

[24] A.L. Gurson. Continuum theory of ductile rupture by void nucleation and growth: Part i – yield criteria and flow rule for porous ductile media. *J. Eng. Mater. Technol., Trans. ASME*, 99(1):2–15, 1977.

[25] Z. Hashin and S. Shtrikman. A variational approach to the theory of the elastic behaviour of multiphase materials. *J. Mech. Phys. Solids*, 11(2):127–140, 1963.

[26] R. Hill. A self-consistent mechanics of composite materials. *J. Mech. Phys. Solids*, 13(4):213–222, 1965.

[27] M. Hintermüller and A. Laurain. Electrical impedance tomography: from topology to shape. *Control Cybern.*, 37(4):913–933, 2008.

[28] M. Hintermüller and A. Laurain. Multiphase image segmentation and modulation recovery based on shape and topological sensitivity. *J. Math. Imaging Vis.*, 35:1–22, 2009.

[29] N. Kikuchi, S. Nishiwaki, J.S.O. Fonseca, and E.C.N. Silva. Design optimization method for compliant mechanisms and material microstructure. *Comput. Methods Appl. Mech. Eng.*, 151(3-4):401–417, 1998.

[30] R. Lakes. Foam structures with negative Poisson's ratio. *Sci., AAAS*, 235(4792):1038–1040, 1987.

[31] R. Lakes. Negative Poisson's ratio materials. *Sci., AAAS*, 238(4826):551, 1987.

[32] I. Larrabide, R.A. Feijóo, A.A. Novotny, and E. Taroco. Topological derivative: a tool for image processing. *Comput. Struct.*, 86(13-14):1386–1403, 2008.

[33] J. Mandel. *Plasticité classique et viscoplasticité*. CISM Lecture Notes. Springer-Verlag, Udine, 1971.

[34] J.C. Michel, H. Moulinec, and P. Suquet. Effective properties of composite materials with periodic microstructure: a computational approach. *Comput. Methods Appl. Mech. Eng.*, 172(1-4):109–143, 1999.

[35] C. Miehe, J. Schotte, and J. Schröder. Computational micro-macro transitions and overall moduli in the analysis of polycrystals at large strains. *Compu. Mater. Sci.*, 16(1-4):372–382, 1999.

[36] S.A. Nazarov and J. Sokołowski. Asymptotic analysis of shape functionals. *J. de Math. Pures Appl.*, 82(2):125–196, 2003.

[37] S. Nemat-Nasser. Averaging theorems in finite deformation plasticity. *Mech. Mater.*, 31(8):493–523, 1999.

[38] S. Nemat-Nasser and M. Hori. *Micromechanics: overall properties of heterogeneous materials*. North-Holland, Amsterdam, 1993.

[39] A.A. Novotny, R.A. Feijóo, E. Taroco, and C. Padra. Topological sensitivity analysis for three-dimensional linear elasticity problem. *Comput. Methods Appl. Mech. Eng.*, 196(41-44):4354–4364, 2007.

[40] S. Osher and J.A. Sethian. Front propagating with curvature dependent speed: algorithms based on Hamilton–Jacobi formulations. *J. Comput. Phys.*, 78:12–49, 1988.

[41] M. Ostoja-Starzewski and J. Schulte. Bounding of effective thermal conductivities of multiscale materials by essential and natural boundary conditions. *Phys. Rev. B*, 54(1):278–285, 1996.

[42] M.L. Oyen, V.L. Ferguson, A.K. Bembey, A.J. Bushby, and A. Boyde. Composite bounds on the elastic modulus of bone. *J. Biomech.*, 41(11):2585–2588, 2008.

[43] E. Sanchez-Palencia. *Non-homogeneous media and vibration theory*, volume 127 of *Lecture Notes in Physics 127*. Springer-Verlag, Berlin, 1980.

[44] O. Sigmund. Materials with prescribed constitutive parameters: an inverse homogenization problem. *Int. J. Solids Struct.*, 31(17):2313–2329, 1994.

[45] E.C.N. Silva, J.S.O. Fonseca, and N. Kikuchi. Optimal design of periodic microstructures. *Comput. Mech.*, 19(5):397–410, 1997.

[46] J. Sokołowski and A. Żochowski. On the topological derivative in shape optimization. *SIAM J. Control Optim.*, 37(4):1251–1272, 1999.
[47] D.C.D. Speirs, E.A. de Souza Neto, and D. Perić. An approach to the mechanical constitutive modelling of arterial tissue based on homogenization and optimization. *J. Biomech.*, 41(12):2673–2680, 2008.
[48] P.M. Suquet. *Elements of homogenization for inelastic solid mechanics*, volume 272 of *Homogenization techniques for composite media, Lecture Notes in Physics 272*. Springer-Verlag, Berlin, 1987.
[49] I. Turevsky, S.H. Gopalakrishnan and K. Suresh. An efficient numerical method for computing the topological sensitivity of arbitrary-shaped features in plate bending. *Int. J. Num. Meth. Engng.*, 79:1683–1702, 2009.
[50] A. Żochowski. Optimal perforation design in 2-dimensional elasticity. *Mech. Struct. Mach.*, 16(1):17–33, 1988.

Topological derivative calculation

For completeness we present here the main steps of the derivation of the topological asymptotic expansion of the homogenized elasticity tensor for topological perturbations in the form of circular inclusions. The derivation presented here offers an alternative to that recently reported in [23] and the final result is an extension of the formula derived in [22] where perturbations in the form of voids were considered instead.

In view of expressions (2.11) and (3.4) we have that the difference between the $ijkl$-components of the tensors $\mathbb{C}^\rho$ and $\mathbb{C}$ is given by:

$$(\mathbb{C}^\rho - \mathbb{C})_{ijkl} = \frac{1}{V_\mu}\int_{\Omega_\mu} \sigma^\rho_\mu(u^\rho_{\mu_{kl}}) \cdot (e_i \otimes e_j) - \frac{1}{V_\mu}\int_{\Omega_\mu} \sigma_\mu(u_{\mu_{kl}}) \cdot (e_i \otimes e_j) \ , \tag{.1}$$

or, by making use of some simple tensorial relations,

$$(\mathbb{C}^\rho - \mathbb{C})_{ijkl} = \frac{1}{V_\mu}\int_{\Omega_\mu} \sigma^\rho_\mu(u^\rho_{\mu_{kl}}) \cdot \nabla^s[(e_i \otimes e_j)y] - \frac{1}{V_\mu}\int_{\Omega_\mu} \sigma_\mu(u_{\mu_{kl}}) \cdot \nabla^s[(e_i \otimes e_j)y] \ . \tag{.2}$$

In view of the additive decomposition (2.13) and (3.6) of the displacement fluctuation fields we have the identities

$$\nabla^s[(e_i \otimes e_j)y] = \nabla^s(u_{\mu_{ij}} - \widetilde{u}_{\mu_{ij}}) = \nabla^s(u^\rho_{\mu_{ij}} - \widetilde{u}^\rho_{\mu_{ij}}) \ , \tag{.3}$$

which replaced back into (.2) yield

$$(\mathbb{C}^\rho - \mathbb{C})_{ijkl} = \frac{1}{V_\mu}\int_{\Omega_\mu} \sigma^\rho_\mu(u^\rho_{\mu_{kl}}) \cdot \nabla^s(u_{\mu_{ij}} - \widetilde{u}_{\mu_{ij}}) - \frac{1}{V_\mu}\int_{\Omega_\mu} \sigma_\mu(u_{\mu_{kl}}) \cdot \nabla^s(u^\rho_{\mu_{ij}} - \widetilde{u}^\rho_{\mu_{ij}}) \ . \tag{.4}$$

By taking into account that both $\widetilde{u}_{\mu_{ij}}$ and $\widetilde{u}^\rho_{\mu_{ij}}$ belong to $\mathcal{U}_\mu$ and making use of the equilibrium equations (2.12) and (3.5) together with the constitutive relations (2.2) and (3.3), expression (.4) reduces to

$$(\mathbb{C}^\rho - \mathbb{C})_{ijkl} = \frac{1}{V_\mu}\int_{\Omega_\mu} \mathbb{C}^\rho_\mu \nabla^s u^\rho_{\mu_{kl}} \cdot \nabla^s u_{\mu_{ij}} - \frac{1}{V_\mu}\int_{\Omega_\mu} \mathbb{C}_\mu \nabla^s u_{\mu_{kl}} \cdot \nabla^s u^\rho_{\mu_{ij}} \ , \tag{.5}$$

or, equivalently, by using the symmetry relation $\mathbb{C}^\rho_\mu \nabla^s u^\rho_{\mu_{kl}} \cdot \nabla^s u_{\mu_{ij}} = \mathbb{C}^\rho_\mu \nabla^s u_{\mu_{ij}} \cdot \nabla^s u^\rho_{\mu_{kl}}$, or $(\mathbb{C})_{ijkl} = (\mathbb{C})_{klij}$,

$$(\mathbb{C}^\rho - \mathbb{C})_{ijkl} = \frac{1}{V_\mu}\int_{\Omega_\mu} [\sigma^\rho_\mu(u_{\mu_{ij}}) - \sigma_\mu(u_{\mu_{ij}})] \cdot \nabla^s u^\rho_{\mu_{kl}} \ . \tag{.6}$$

Finally, by taking into account the definitions of the original and perturbed microscopic domains and their corresponding constitutive relations, the above expression can be equivalently written in terms of an integral over the perturbation $\mathcal{I}_\rho$:

$$(\mathbb{C}^\rho - \mathbb{C})_{ijkl} = \frac{\gamma - 1}{V_\mu}\int_{\mathcal{I}_\rho} \sigma_\mu(u_{\mu_{ij}}) \cdot \nabla^s u^\rho_{\mu_{kl}} \ . \tag{.7}$$

The first order asymptotic expansion of the above quantity for an arbitrarily shaped inclusion can be obtained in a similar way as in [3]. The present problem, however, differs from that of [3] in the functional spaces and boundary conditions involved. Thus we briefly present in what follows the main steps of the derivation. For simplicity we restrict ourselves to circular inclusions. We start by re-writting (.7) in the equivalent form

$$(\mathbb{C}^\rho - \mathbb{C})_{ijkl} = \frac{\gamma - 1}{V_\mu}\left[\int_{\mathcal{I}_\rho} \sigma_\mu(u_{\mu_{ij}}) \cdot \nabla^s u_{\mu_{kl}} + \int_{\mathcal{I}_\rho} \sigma_\mu(u_{\mu_{ij}}) \cdot \nabla^s (u^\rho_{\mu_{kl}} - u_{\mu_{kl}})\right] , \tag{.8}$$

and then replace the first integral with an approximation to obtain

$$(\mathbb{C}^\rho - \mathbb{C})_{ijkl} = \frac{\gamma - 1}{V_\mu}\left[\pi\rho^2\sigma_\mu(u_{\mu_{ij}})(\widehat{y})\cdot\nabla^s u_{\mu_{kl}}(\widehat{y}) + \mathcal{E}_1(\rho) + \int_{\mathcal{I}_\rho}\sigma_\mu(u_{\mu_{ij}})\cdot\nabla^s(u^\rho_{\mu_{kl}} - u_{\mu_{kl}})\right]. \qquad (.9)$$

Here and in what follows $\mathcal{E}_i(\rho)$ denotes remainders whose behavior will be discussed later. Now we consider the solution $\sigma^\rho_\mu(w^\rho_{kl})$ of the exterior problem defined by

$$\left\{\begin{array}{rcll} -\text{div}\,(\sigma^\rho_\mu(w^\rho_{kl})) &=& 0 & \text{in}\quad \mathcal{I}_\rho \cup (\mathbb{R}^2 \setminus \overline{\mathcal{H}_\rho})\,, \\ [\![\sigma^\rho_\mu(w^\rho_{kl})]\!]n &=& -(1-\gamma)\sigma_\mu(u_{\mu_{kl}})(\widehat{y})n & \text{on}\quad \partial\mathcal{I}_\rho\,, \\ \sigma^\rho_\mu(w^\rho_{kl}) &\to& 0 & \text{at}\quad \infty\,, \end{array}\right. \qquad (.10)$$

where $[\![(\cdot)]\!]$ denotes the jump of the function $(\cdot)$ across the matrix/inclusion interface $\partial\mathcal{I}_\rho$:

$$[\![(\cdot)]\!] := (\cdot)|_m - (\cdot)|_i\,, \qquad (.11)$$

with subscripts m and i associated with quantities evaluated on the matrix and inclusion boundaries, respectively. Then, by considering the symmetry of the constitutive tensor in (2.2) and taking the solution of (.10) as an esimate for the variation $\sigma^\rho_\mu(u^\rho_{\mu_{kl}} - u_{\mu_{kl}})$, we obtain the following for the rightmost integral in (.8)

$$\begin{aligned} \int_{\mathcal{I}_\rho}\sigma_\mu(u_{\mu_{ij}})\cdot\nabla^s(u^\rho_{\mu_{kl}} - u_{\mu_{kl}}) &= \int_{\mathcal{I}_\rho}\nabla^s u_{\mu_{ij}}\cdot\sigma_\mu(u^\rho_{\mu_{kl}} - u_{\mu_{kl}}) \\ &= \int_{\mathcal{I}_\rho}\nabla^s u_{\mu_{ij}}\cdot\sigma_\mu(w^\rho_{\mu_{kl}}) + \mathcal{E}_2(\rho) \\ &= \nabla^s u_{\mu_{ij}}(\widehat{y})\cdot\int_{\mathcal{I}_\rho}\sigma_\mu(w^\rho_{kl}) + \mathcal{E}_2(\rho) + \mathcal{E}_3(\rho), \end{aligned} \qquad (.12)$$

where an extra approximation involving $\nabla^s u_{\mu_{ij}}$ has been introduced to arrive at the third right hand side.

In the present case of a circular inclusion, the nominal stress tensor $\sigma_\mu(w^\rho_{kl})$ has the following representation in a polar coordinate system (r,θ) with origin at the center $\widehat{y}$ of the inclusion:

- for $r \geq \rho$

$$\sigma^r_\mu(r,\theta) = -\frac{1}{2}(\sigma^I_\mu + \sigma^{I\!I}_\mu)\frac{1-\gamma}{1+\alpha\gamma}\frac{\rho^2}{r^2} - \frac{1}{2}(\sigma^I_\mu - \sigma^{I\!I}_\mu)\frac{1-\gamma}{1+\beta\gamma}\left(4\frac{\rho^2}{r^2} - 3\frac{\rho^4}{r^4}\right)\cos 2\theta\,, \qquad (.13)$$

$$\sigma^\theta_\mu(r,\theta) = \frac{1}{2}(\sigma^I_\mu + \sigma^{I\!I}_\mu)\frac{1-\gamma}{1+\alpha\gamma}\frac{\rho^2}{r^2} - \frac{3}{2}(\sigma^I_\mu - \sigma^{I\!I}_\mu)\frac{1-\gamma}{1+\beta\gamma}\frac{\rho^4}{r^4}\cos 2\theta\,, \qquad (.14)$$

$$\sigma^{r\theta}_\mu(r,\theta) = -\frac{1}{2}(\sigma^I_\mu - \sigma^{I\!I}_\mu)\frac{1-\gamma}{1+\beta\gamma}\left(2\frac{\rho^2}{r^2} - 3\frac{\rho^4}{r^4}\right)\sin 2\theta\,; \qquad (.15)$$

- for $0 < r < \rho$

$$\sigma^r_\mu(r,\theta) = \frac{1}{2}(\sigma^I_\mu + \sigma^{I\!I}_\mu)\frac{1-\gamma}{1+\alpha\gamma}\alpha + \frac{1}{2}(\sigma^I_\mu - \sigma^{I\!I}_\mu)\frac{1-\gamma}{1+\beta\gamma}\beta\cos 2\theta\,, \qquad (.16)$$

$$\sigma^\theta_\mu(r,\theta) = \frac{1}{2}(\sigma^I_\mu + \sigma^{I\!I}_\mu)\frac{1-\gamma}{1+\alpha\gamma}\alpha - \frac{1}{2}(\sigma^I_\mu - \sigma^{I\!I}_\mu)\frac{1-\gamma}{1+\beta\gamma}\beta\cos 2\theta\,, \qquad (.17)$$

$$\sigma^{r\theta}_\mu(r,\theta) = -\frac{1}{2}(\sigma^I_\mu - \sigma^{I\!I}_\mu)\frac{1-\gamma}{1+\beta\gamma}\beta\sin 2\theta\,, \qquad (.18)$$

where σ^I_μ and $\sigma^{I\!I}_\mu$ are the eigenvalues of the tensor $\sigma_\mu(u_{kl})(\widehat{y})$. In addition, the constants α and β are given respectively by

$$\alpha = \frac{1+\nu_\mu}{1-\nu_\mu}\,, \qquad \beta = \frac{3-\nu_\mu}{1+\nu_\mu}\,. \qquad (.19)$$

Representation (.13)–(.18) for the nominal stress $\sigma_\mu(w^\rho_{kl})$ allows the integral term in (.12) to be analytically calculated and resuts in

$$\int_{\mathcal{I}_\rho}\sigma_\mu(w^\rho_{kl}) = -\pi\rho^2\zeta\mathbb{T}\sigma_\mu(u_{\mu_{kl}})(\widehat{y})\,, \qquad (.20)$$

with the scalar value ζ and the fourth order tensor $\mathbb{T}$ given by

$$\zeta = -\frac{1-\gamma}{1+\beta\gamma} \quad \text{and} \quad \mathbb{T} = \beta\mathbb{I} + \frac{1}{2}\frac{\alpha-\beta}{1+\gamma\alpha}\mathrm{I}\otimes\mathrm{I}\,. \tag{.21}$$

By replacing (.20) in (.12) and then substituting the result into (.9), we finally arrive at the following estimate for the difference between the $ijkl$-components of the homogenized elasticity tensors $\mathbb{C}^\rho$ and $\mathbb{C}$ of the perturbed and original RVEs:

$$\begin{aligned}(\mathbb{C}^\rho - \mathbb{C})_{ijkl} \quad &= \quad \frac{\pi\rho^2}{V_\mu}(1-\gamma)\zeta\left\{\frac{1+\beta}{1-\gamma}\sigma_\mu(u_{\mu_{kl}})\cdot\nabla^s u_{\mu_{ij}} + \frac{1}{2}\frac{\alpha-\beta}{1+\gamma\alpha}\mathrm{tr}[\sigma_\mu(u_{\mu_{kl}})]\mathrm{tr}(\nabla^s u_{\mu_{ij}})\right\}(\widehat{y}) \\ &\quad +(\gamma-1)\sum_{i=1}^{3}\mathcal{E}_i(\rho)\,. \end{aligned} \tag{.22}$$

By following analogous steps to those of [3] it can be shown that

$$\sum_{i=1}^{3}\mathcal{E}_i(\rho) = o(\rho^2). \tag{.23}$$

Then, by comparing (.22,.23) with the topological asymptotic expansion (3.7) we identify the function f according to (3.8) and the topological derivative of the tensor $\mathbb{C}$ as

$$(D_T\mathbb{C})_{ijkl} = (1-\gamma)\zeta\left(\frac{1+\beta}{1-\gamma}\sigma_\mu(u_{\mu_{kl}})\cdot\nabla^s u_{\mu_{ij}} + \frac{1}{2}\frac{\alpha-\beta}{1+\gamma\alpha}\mathrm{tr}(\sigma_\mu(u_{\mu_{kl}}))\mathrm{tr}(\nabla^s u_{\mu_{ij}})\right) \tag{.24}$$

with α and β given by (3.11). The topological derivative of $\mathbb{C}$ can be expressed in compact form by (3.9).

(S. Amstutz) Laboratoire d'analyse non linéaire et géométrie, Faculté des Sciences, 33 rue Louis Pasteur, 84000 Avignon, France.
Email address: samuel.amstutz@univ-avignon.fr

(S.M. Giusti) Laboratório Nacional de Computação Científica LNCC/MCT, Coordenação de Matemática Aplicada e Computacional, Av. Getúlio Vargas 333, 25651-075, Petrópolis - RJ, Brasil
Email address: giusti@lncc.br

(A.A. Novotny) Laboratório Nacional de Computação Científica LNCC/MCT, Coordenação de Matemática Aplicada e Computacional, Av. Getúlio Vargas 333, 25651-075 Petrópolis - RJ, Brasil.
Email address: novotny@lncc.br

(E.A. de Souza Neto) Civil and Computational Engineering Centre, School of Engineering, Swansea University, SingletonPark, Swansea SA28PP, UK
Email address: E.deSouzaNeto@swansea.ac.uk